# Synthetic, physical and computational chemistry of propeller-shaped polycyclic aromatic hydrocarbons

Ham, A. van der

# Chapter 3

## Conformational Behavior and Spectroscopic Properties of a Pyrene-based π-extended Triple Helicene

Abstract

The previous Chapter described the synthesis of tripyrenylene. This Chapter will start by analysing its conformational behaviour using variable temperature NMR. The different conformational isomers of the propellerene are then separated and their spectroscopic properties studied and compared to other helicenes and propellerenes. The effect an increase in the π-conjugated system has on the physico-chemical properties of helicene molecules is studied and, in particular, whether the location of π-extension is of importance or not. It is shown that tripyrenylene exhibits behaviour very similar to other (π-extended) propellerenes, suggesting the location of the π-extension to be of lesser importance than the π-extension itself. It also indicates that the properties of multiple helicenes are dictated by the helical motif itself. Using DFT computations, the similarities between the different helicenes and propellerenes are traced back to the molecular orbital level.

Parts of this Chapter are published as:
van der Ham A., Hansen T., Brouwer A. M., Overkleeft H. S., Hamlin T., Filippov D. V., Schneider G. F. **Manuscript in preparation.** Pre-print available (doi: 10.26434/chemrxiv-2021-kn2qg)

One striking characteristic property of aromatic molecules is their ability to absorb and emit light in the ultraviolet (UV) and visible range (~200 – 800 nm). Absorption of light takes place when the light shone onto a molecule is able to excite an electron from an occupied orbital to an unoccupied orbital; emission takes place when the excited electron falls back to its original, ground state. Because π electrons are less tightly bound than sigma electrons, they are more easily excited (π → π*), requiring less energy to do so, and thus absorption takes place at longer wavelengths. When π electrons are delocalized in a conjugated system, this energy gap becomes even smaller, resulting in absorption taking place at ever longer wavelengths. Because the optical properties of aromatic molecules are thus driven by the size of their conjugated system, the relationship between these two factors provides an important guiding principle for the design of PAH-based photo-optical materials.[2-4] Yet, although such relationships have been well documented for monohelicenes[7,8] and multiple helicenes,[10] a systematic study on the effects of π-extension on the physicochemical properties of helicenes *vis-à-vis* propellerenes appears absent in the literature.

An initial comparison of the reported UV-Vis spectra of [5]helicene (**5H**),[1] dibenzo[*f,j*]picene (**DBP**),[5] hexabenzotriphenylene-$C_2$ (**HBT-$C_2$**) and Kamikawa *et al.*'s hexapole [5]helicene-$C_2$ (**HH-$C_2$**) shows that an increase in the size of the aromatic system is associated with an, expected, bathochromic broadening of the absorption curve, with the absorption onset shifting from ~370 to 500 nm (Fig. 3.1). A number of conserved absorption features can be discerned in all spectra. A global absorption maximum close to 250 nm is observed, with **5H** and **DBP** showing two local maxima centered around 300 nm (dotted line), which are red shifted for **HBT-$C_2$** and **HH-$C_2$** to 350 and 390 nm respectively. All spectra also show a distinctive shoulder in the absorption onset, which broadens and shifts from 330 nm for **5H** to 450 nm for **HH-$C_2$**. Before tripyrenylene **1**, prepared in the preceding Chapter, can be compared to this list, its exact structure first needs to be defined. As explained in Chapter 1, what differentiates propellerenes from other helicene derivatives, is that they can adopt two distinct conformations: a $C_2$ and $D_3$ conformation, depending on the relative orientation of the wings, and the resultant molecular symmetry. Apart from these two conformations, each conformation exists as a pair of enantiomers, which are non-superimposable mirror images of one another (Scheme 3.1). In the previous chapter, analysis of the conformation in which **1** was isolated was purposefully foregone. This issue will therefore be addressed here first.

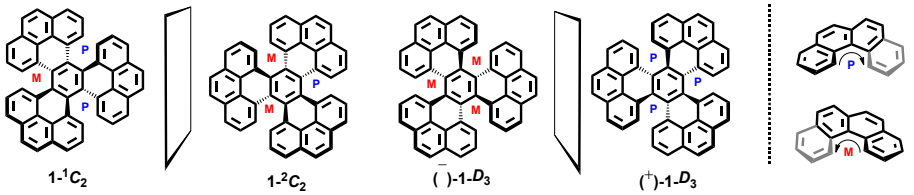


**1-$^1C_2$** **1-$^2C_2$** **(⁻)-1-$D_3$** **(⁺)-1-$D_3$**

**Scheme 3.1** Structures of the two enantiomers of **1**-$C_2$ and **1**-$D_3$, with the chirality of the helical motifs labelled.

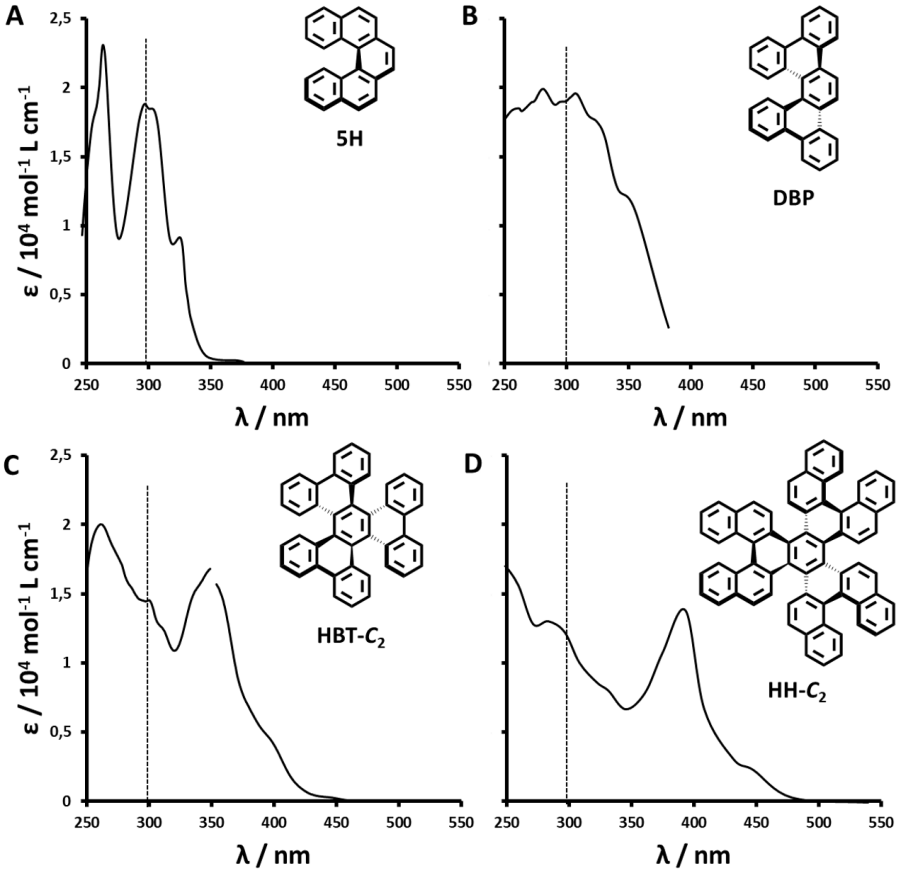


**Figure 3.1** Experimental UV-Vis spectra of (A) [5]helicene,[1] (B) dibenzopicene[5] and (C) HH-$C_2$[6], recreated from those originally reported.[9] Spectrum of HBT-$C_2$ (D) was recorded in this work. Absorptions are arbitrarily scaled. Dotted line added at 300 nm for ease of reference.

*VT NMR*. One of the most straightforward methods of determining the conformation in which a propellerene resides is by variable temperature (VT) NMR spectroscopy (Fig. 3.3A). At room temperature, the $^1$H spectrum of **1** only shows four resonances due to rapid interconversion between the two $C_2$ conformations (Fig. 3.2 and Fig. 3.4). When cooled to –100°C, however, interconversion is no longer possible and a dramatic change in the spectrum is observed, with the emergence of additional resonances corresponding to individual protons on **1**-$C_2$ (note that the two conformers are both chemically and magnetically equivalent and thus their resonances coincide). The coalescence temperature for the interconversion between the two $C_2$ conformers was found to be approximately –90 °C, corresponding to a barrier height to interconversion of 10.0 kcal mol$^{-1}$, which is close to the computed value of 9.9 kcal mol$^{-1}$ (Fig. 3.3B). Heating of the solution to 80 °C resulted in conversion to the $D_3$ conformation. This was evidenced by the disappearance of the $C_2$ resonances, with a half time of approximately 20 mins., corresponding to a barrier height of $\Delta G^{\ddagger}$ = 26.0 kcal mol$^{-1}$, and which is in excellent agreement with the computed value of 26.4 kcal mol$^{-1}$. When the solution was again cooled to –80 °C, only an insignificant change in chemical shift was observed but no change in the number or multiplicity of the resonances. This confirmed **1** to now reside in the $D_3$ conformation, which was further verified by recording VT NMR spectra of the isolated conformers in different solvents (Fig. 3.4).

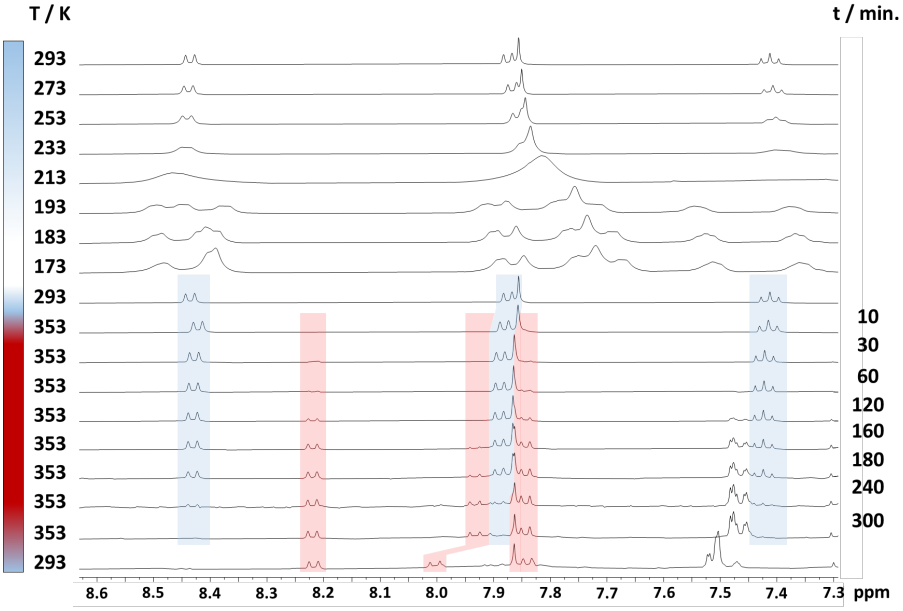


**Figure 3.2** $^1$H VT-NMR spectra of **1** in Tol-$d_8$. Spectra are arbitrarily scaled for clarity. Multiplets around 7.5 ppm originate from the solvent. Resonances shaded in blue and red belong to the $C_2$ and $D_3$ conformer respectively. Observed is a dramatic change in resonances upon cooling of **1** in the $C_2$ conformer, and a gradual disappearance of the $C_2$ resonances and appearance of resonances of the $D_3$ conformer when the solution is heated to 100 °C.

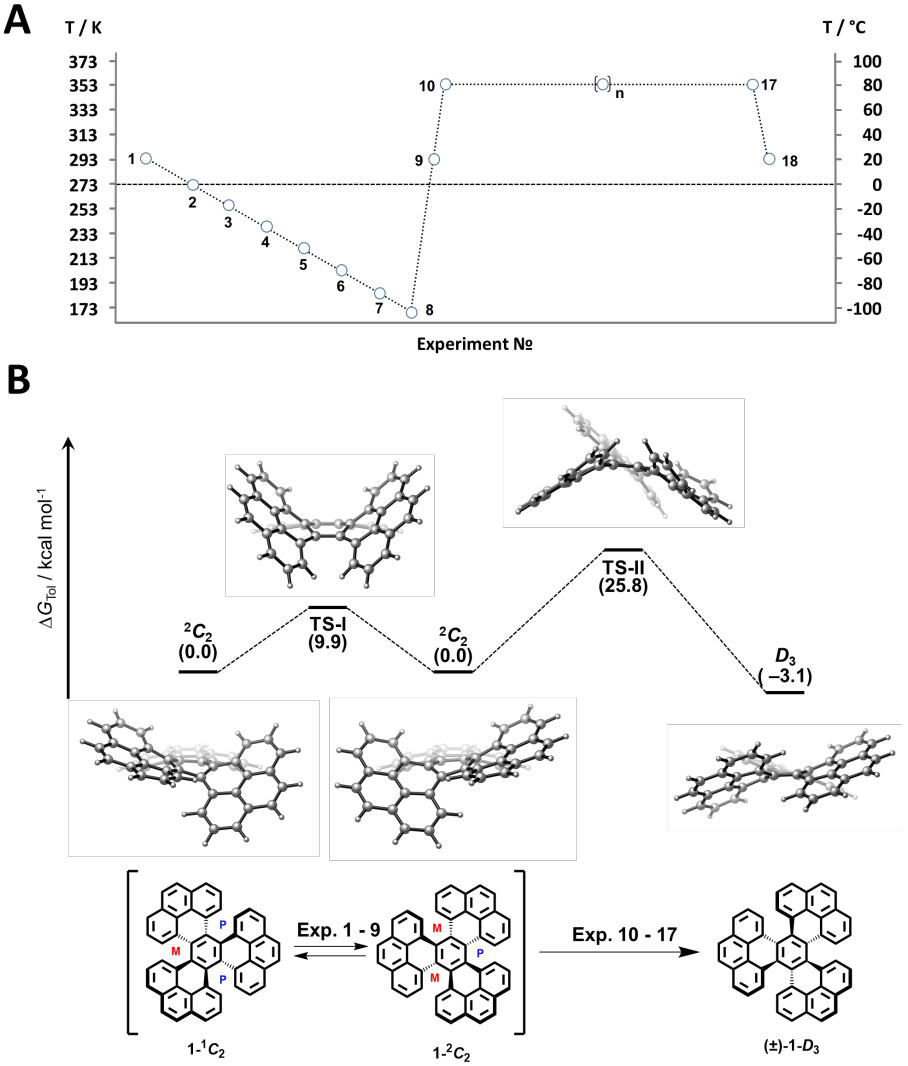


**Figure 3.3** (A) Temperature profile of the VT-NMR experiment shown in Fig. 3.2. (B) Potential energy surface for the interconversion of **1** between its $C_2$ and $D_3$ conformations. Gibbs free energies (in kcal mol$^{-1}$) were computed at the SMD(Toluene)-PBE-D3(BJ)/6-31G(d,p) level. Indicated are which processes take place at which points during the VT NMR experiment.

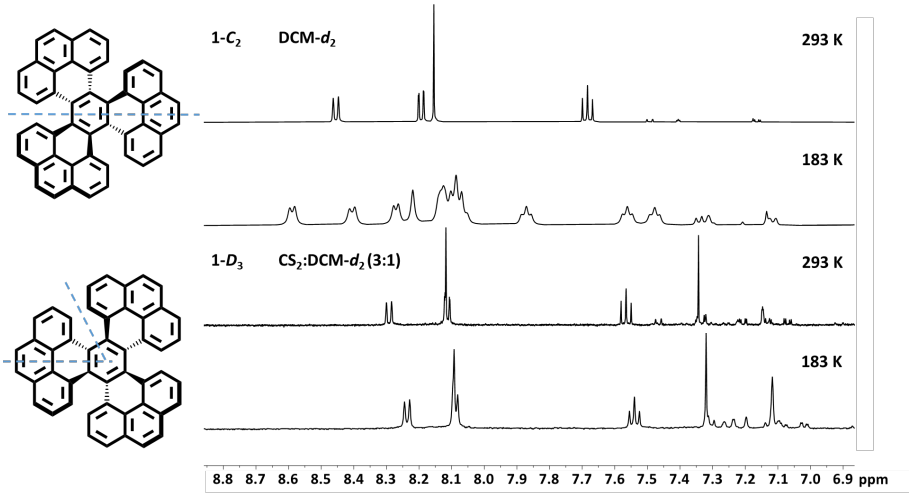


**Figure 3.4** Reference $^1$H VT-NMR spectra of the $C_2$ and $D_3$ conformer of **1** in DCM-$d_2$ and $CS_2$:DCM-$d_2$ (3:1) respectively. Signals in the spectrum of **1**-$D_3$ upfield of 7.5 ppm originate from impurities in the solvent. Blue dashed lines indicate the symmetry axes of the propellerenes.

It is of interest to note that, during the $C_2 \rightarrow D_3$ conversion at 80 °C, the compound was found to precipitate out of solution. This indicates that the $D_3$ conformer of tripyrenylene is significantly less soluble than the $C_2$ conformer. Computationally, the dimerization energies of the $C_2$ and $D_3$ conformer were indeed found to be –21.9 and –24.4 kcal mol$^{-1}$ respectively, corroborating this observation. This observation can be attributed to a much better stacking of the $D_3$ conformer, due to its lesser degree of contortion from planarity compared to the $C_2$ conformer. Indeed, the intermolecular distances were found to be 4.50 and 4.40 Å for the $C_2$ and $D_3$ dimer respectively (Fig. 3.5).

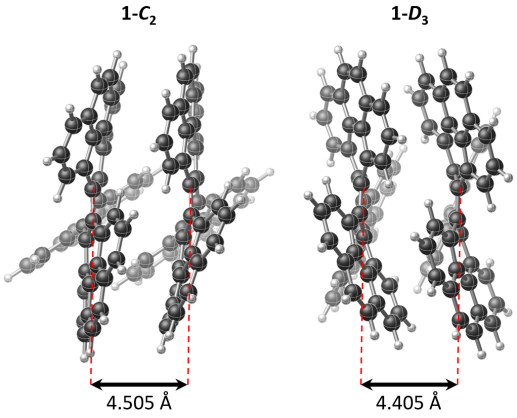


**Figure 3.5** Computed gas-phase geometries of the **1**-$C_2$ and **1**-$D_3$ dimer, showing the intercore distance. The shortest intermolecular C — C distance was approximately 3.37 Å for both structures.

*Palladium catalyzed [2+2+2] aryne cyclotrimerization.* What the NMR experiments show is that tripyrenylene **1** was synthesized as the $C_2$ conformer, even though the DFT computations indicated that this conformer is thermodynamically less favorable than the $D_3$ conformer (Fig. 3.3A). Although surprising at first, this is actually in agreement with the fact that the palladium(0) catalyzed [2+2+2] cycloaddition of arynes is known to proceed under kinetic control.[11-13]

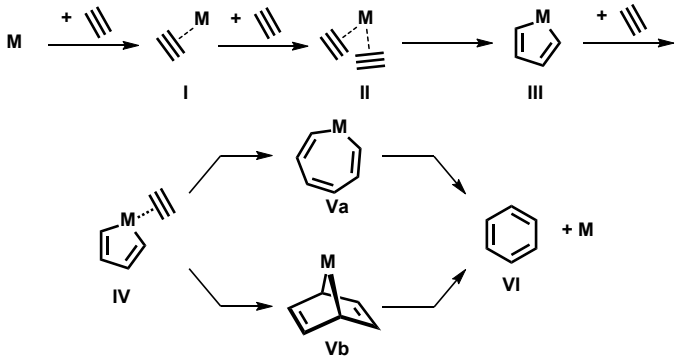


**Scheme 3.2** General reaction scheme for the [2 + 2 + 2] cycloaddition of three alkynes, catalyzed by a transition metal **M**. Substituents on the alkynes and (solvent) ligands on the metal center were omitted for clarity. Adopted from: ,,Mechanistic Studies of Transition-Metal-Catalyzed [2 + 2 + 2] Cycloaddition Reactions" (Ref. 9).

The general reaction scheme for the [2 + 2 + 2] cycloaddition of three alkynes is given in Scheme 3.2. In short, the reaction starts with the barrierless coordination of two alkyne units to the metal center (**I** and **II**), which then combine to give diene **III**. Note that this reaction is only barrierless when disregarding solvents or ligands coordinating to the metal center. Gibbs free energies of association and dissociation of solvent molecules and ligands are typically on the order of 1 – 2 kcal $mol^{-1}$ and –10 – +20 kcal $mol^{-1}$, respectively.[14,15] Coordination of a third alkyne then gives metallocomplex **IV**. Insertion of the third alkyne typically proceeds *via* one of two possible mechanisms: in a two-step fashion *via* a seven-membered intermediate (**Va**), known as the Schore mechanism;[16] or in a concerted [4 + 2] cycloaddition fashion, *i.e.* a canonical Diels-Alder reaction (**Vb**).[17] Reductive elimination of the metal then regenerates the catalyst, and yields the final, aromatic product **VI**. Yet, despite the plethora of computational studies related to the transition metal catalyzed coupling of alkynes, the corresponding reaction of arynes is much less studied.[18] To understand at which point in the reaction kinetic control over the reaction is exerted, and whether this control is substrate dependent or independent, the entire potential energy surface (PES) of this reaction was computed.

In view of the computational cost associated with large systems, the PES of the [2+2+2] cycloaddition of benzyne, which yields the planar triphenylene, was computed first (Fig. 3.6A). This was then extended to the phenanthren-4,5-yne system which yields hexabenzotriphenylene (HBT; Fig. 3.6B), for which the steric control of this reaction was first reported. PESs were computed at the SMD($CHCl_3$)-PBE-D3(BJ)/6-31G(d,p) level, and both the benzyne and phananthryne reactions were found to proceed in a similar fashion, starting with the step-wise coordination of two aryne units to a single palladium(0) atom. A palladacyclic intermediate **B3**/**P3** is then formed *via* a transition state **TS-I**. In the case of benzyne, the intermediate **B3** has a planar $C_{2v}$ symmetry,[19] whereas steric clash between the spatially proximal rings in palladacycle **P3** results in the adaptation of a non-planar geometry. Coordination of a third aryne to the palladium center in diene **B3**/**P3** results in a further lowering in free Gibbs energy, yielding reaction intermediates **B4**/**P4**. It is of interest to note that this final aryne unit is oriented orthogonal to the diene plane. This geometrical feature is observed only when dispersion is accounted for (*i.e.* when using ωB97X-D or PBE-D3(BJ) as functionals). When no dispersion correction is applied (*i.e.* uncorrected B3LYP) the aryne ring is centered on the Pd atom, *i.e.* yielding a $D_2$ symmetry in the case of benzyne (Fig. S3.1). Although not directly comparable, a similar non-symmetrical structure was found both experimentally and computationally for the $V^+(C_4H_4)\cdots(C_2H_2)$ complex.[20] For both **B4** and **P4**, transition states could only be located for insertion of the final aryne *via* a Schore mechanism (**TS-II**). As reported before by others,[6] it was not possible to locate a TS that describes a concerted [4 + 2] cycloaddition, *i.e.* a canonical Diels-Alder addition. To prove that such a concerted mechanism is much less favorable, a constrained PES can be constructed in which bond forming C···C distances are artificially constrained to be synchronously concerted (Fig. S3.2). Although the initial products of both PESs are different, the energetic maximum of the concerted synchronous reaction is approximately 25 kcal $mol^{-1}$ more endergonic with respect to the TS of the step-wise addition (*i.e.* **TS-II**). This is attributable to a much less favorable orbital alignment, steric clash and the requirement for an unfavorable dearomatization of the palladacyclic complex. The $C_2$ symmetry of **B5** and **P5** is introduced at this point along the reaction coordinate and is retained after ring closure *via* a low energy barrier (**TS-III**). Based on this finding, it can be concluded that the kinetic control of this reaction is substrate independent.

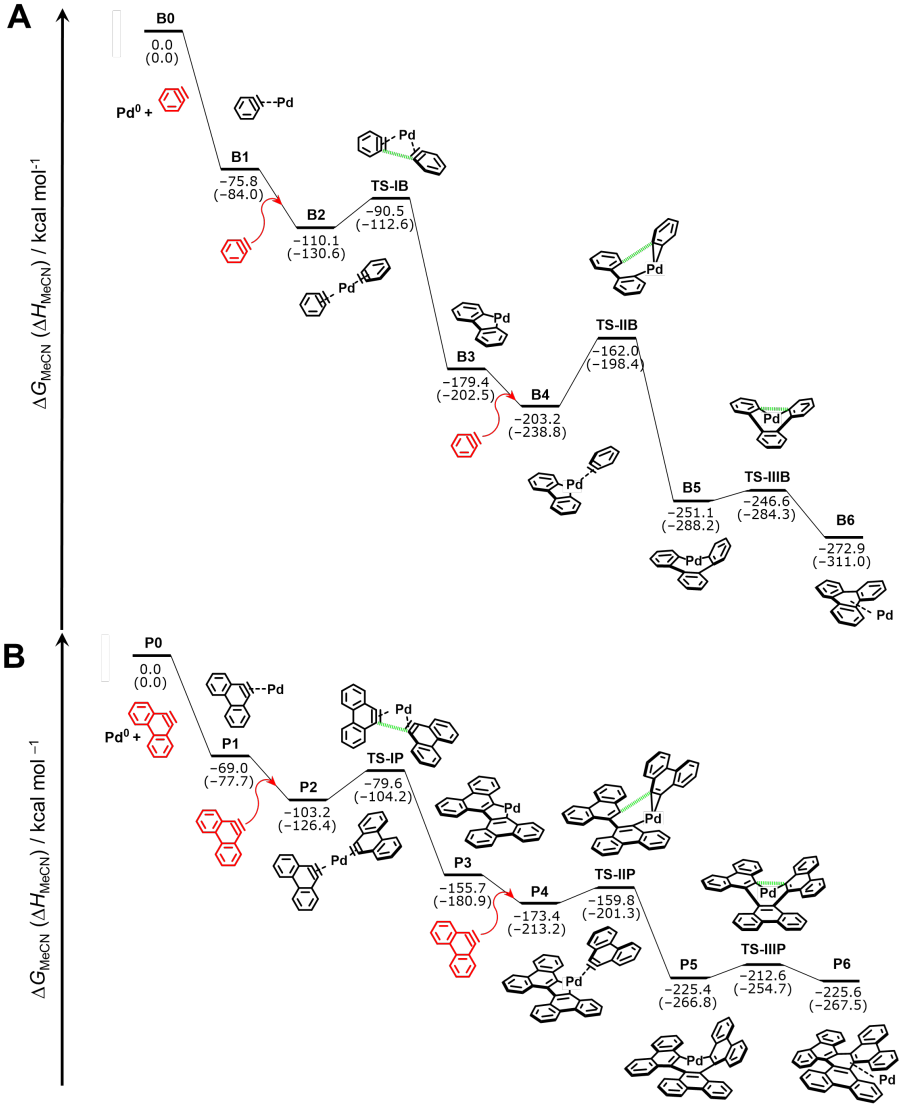


**Figure 3.6** The potential energy surface of the palladium(0) catalyzed trimerization of benzyne (A) and phenanthren-9,10-yne (B). Gibbs free energies and enthalpies are computed at the SMD(MeCN)-PBE-D3(BJ)/6-31G(d,p) level of theory are given in kcal $mol^{-1}$.

*UV-Vis Spectroscopy*. Because interconversion of the $C_2$ conformer to the $D_3$ conformer is sufficiently slow at room temperature, combined with the fact that the $D_3$ conformer is thermodynamically preferred to a significant degree (Fig. 3.3), the isomers can be separated and their photo-optical properties studied separately.[21]

The UV-Vis spectrum of a solution of **1**-$C_2$ in chloroform shows an absorption onset at 504 nm, corresponding to an optical band gap of 2.46 eV (Fig. 3.7). Weak shoulders are observed at 439 nm and 416 nm, which were computed using time dependent (TD) DFT at B3LYP/6-311+G(2d,p)//B3LYP-D3(BJ)/6-31G(d,p) to correspond to the HOMO → LUMO transition, and a mixture of different frontier orbital transitions ($\lambda_{calc}$ = 451 nm, $f$ = 0.0606; $\lambda_{calc}$ = 424 nm, $f$ = 0.0097) (Table S3.2). Two local maxima are found at 385 nm and 365 nm, with a global maximum located at 295 nm ($\varepsilon_{max,C2}$ = 3.05 x $10^4$ $mol^{-1}$ L $cm^{-1}$). The spectrum of **1**-$D_3$ is distinctly different to that of **1**-$C_2$. The absorption onset is slightly red shifted compared to that of **1**-$C_2$ at 522 nm, corresponding to an optical band gap of 2.37 eV. Absorption bands are found at 506 nm and 473 nm, corresponding respectively to the HOMO → LUMO +1 ($\lambda_{calc}$ = 482 nm, $f$ = 0.0000) and a mixed HOMO → LUMO / HOMO –1 → LUMO +1 ($\lambda_{calc}$ = 445 nm, $f$ = 0.0264) transition. A single local maximum is found at 394 nm with the global maximum located at 282 nm ($\varepsilon_{max,D3}$ = 2.83 x $10^4$ $mol^{-1}$ L $cm^{-1}$). Comparison of the UV-Vis spectra of **1** to that of **HBT** (Fig. 3.7) and **HH** (Fig. 3.1) in the same solvent shows, apart from a bathochromic shift and broadening, a near identical band pattern.[6] This provides an initial hint that, although increased conjugation results in a change in photo-optical properties, the exact location at which this increased conjugation is introduced is only of nominal importance.

Recording of the emission spectrum of **1**-$D_3$, when excited at the 394 nm band revealed, apart from the expected mirror image of the absorption spectrum, a minor emission band around 400 nm, ahead of a main emission band around 515 nm (Fig. 3.8A). Recording of a 2D excitation/emission spectrum revealed the origin of the 400 nm emission to originate from an absorption feature at 350 nm (Fig. S3.4). It was initially speculated that this feature was indicative of excimer formation.

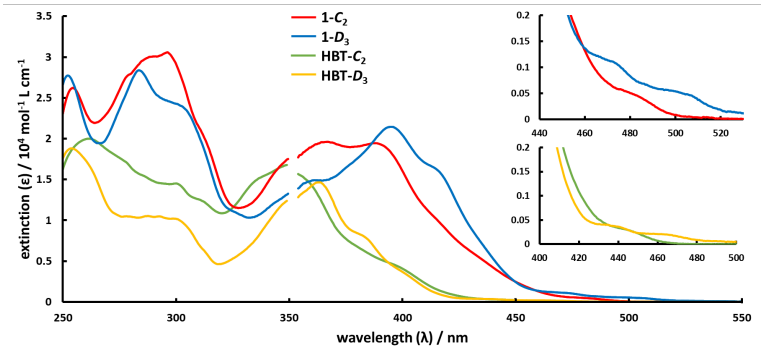


**Figure 3.7** UV-Vis spectra of **HBT** and **1** recorded as solutions in chloroform at room temperature. The gap around 350 nm is due to switching of the lamp. Insets show the separate absorption onsets of the tripyrenylenes (top) and HBT (bottom).

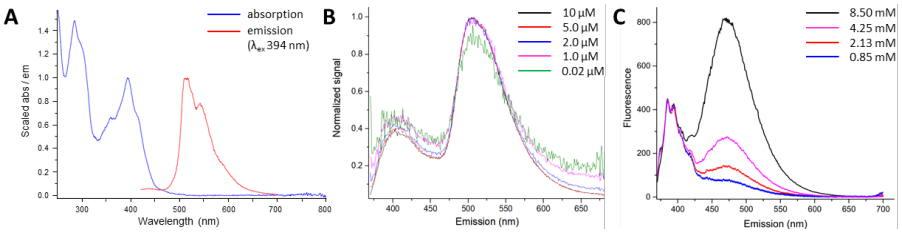


**Figure 3.8** (A) Absorption/emission spectrum of **1**-$D_3$ (*n*-heptane:$CHCl_3$, $c \approx 1 \cdot 10^{-5}$ M). (B) Dilution array fluorescence spectra of **1**-$D_3$ in *n*-heptane, excited at 350 nm. Emission normalized to the feature around 520 nm. (C) Dilution array fluorescence spectrum of pyrene in *n*-heptane excited at 350 nm. Normalized to the emission around 400 nm. Note the change in relative intensity of the maxima around 400 and 475, which is not observed for the features in **1**-$D_3$.

The concept of excimer formation is best illustrated using the parent pyrene molecule. Pyrene itself is well-known to form excimers in solution, giving rise to a broad, featureless emission at around 500 nm (also see Fig. 3.8C).[22-25] Excimers (E) are formed when a ground state ($S_0$) monomeric molecule (M) is excited to a higher energy exited state ($S_1$, M*) and then associates with another, ground state, molecule (Fig. 3.9A).[26-28] The pyrene excimer complex is geometrically distinct from the ground state pyrene dimer (D) and its excited counterpart (D*). Namely, whereas the excimer complex adopts a sandwich configuration, the ground state and excited pyrene dimer adopt slipped-parallel configurations.[27] Thus, upon relaxation of the excimer complex, a state will be reached which is higher in energy than the ground state dimer (D), and indeed does not constitute a stationary point on the PEL (Fig. 3.9A). The stabilization of the excimer has traditionally been attributed to exciton resonance, whereby the excitation energy is delocalized over both components of the excimer complex, and light will therefore be emitted from the excimer at a longer wavelength than from the monomer; *i.e.* $h\nu^{e}_{em} < h\nu^{m}_{ex/em}$ (Fig. 3.8A).[22]

The presence of dimeric excimer formation can be experimentally verified by recording the excitation/emission spectrum at different substrate concentrations. At lower concentrations, less dimer formation and thus excimer formation is expected, and which is shown for pyrene in Figure 3.8C. For **1**, however, the relative intensity of the emissions at 400 and 520 nm remains invariant with concentration, suggesting the formation of an *intramolecular excimer*. In other words, irradiation of **1** can lead to formation of an excited **1$^{1}$*** species which emits light at a particular wavelength ($h\nu^{1*}_{em}$, $\lambda \approx 400$ nm). However, within **1**, the enforced close proximity of the pyrene units also allows adjacent wings to couple to one another, *i.e.* form an intramolecular excimer, which emits light of lower energy ($h\nu^{2*}_{em}$, $\lambda \approx 520$ nm; Fig. 3.9B). Examples of intramolecular excimer formation are known for several PAHs in the literature.[29-32] To prove this hypothesis, time-resolved fluorescence experiments can be performed. As formation of the excimer requires diffusion an excited molecule to a ground state molecule, one would expect a delayed emission after the excitation event. If indeed found, these results would constitute the first, indirect, experimental proof that the

central ring of (benzoid) propellerenes are not conjugated (*i.e.* do not constitute a classical Clar sextet), which has thus far only been inferred computationally.[33-37] These experiments are currently underway. Other possible explanations for the observed emission pattern are the presence of minor, but strongly emitting, impurities or; preferential excitation of higher energy states (*i.e.* a violation of Kasha's rule).

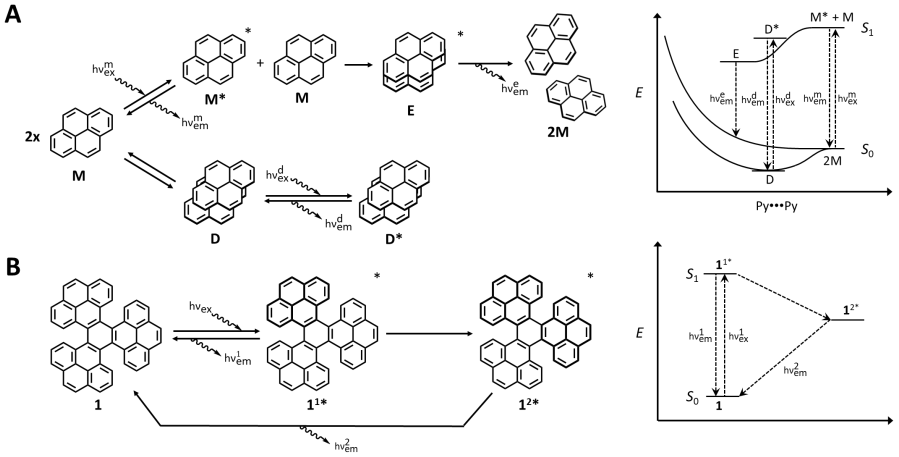


**Figure 3.9** Schematic overview of the formation of pyrene eximers (A) and intramolecular eximer formation in **1** (B). Schematic potential energy diagrams for both processes are given to the right. For pyrene the PES is plotted as a function of the intermolecular distance.

*Frontier Orbitals.* The similarity in absorption-emission spectra between the different propellerenes suggests that the underlying molecular orbital structure is also similar. The frontier molecular orbitals (FMOs) of both conformers of **1** and **HBT** were therefore computed using TD-DFT at B3LYP/6-311+G(2d,p)//B3LYP-D3(BJ)/6-31G(d,p), (which was first verified on **5H** (Table S3.1)), and compared to those reported for **HH**.[6] The HOMOs and LUMOs of **1** in both conformations are largely of an expected π and π*-type, respectively. The HOMO/HOMO –1 and LUMO/LUMO +1 pairs are distinguishable by the pattern of the MOs on the wings of the propellerenes (Fig. 3.10). This feature allows tracking of the frontier orbitals during the $C_2 \rightarrow D_3$ conversion. It is observed that, during this transition, the HOMO of **1**-$C_2$ becomes more stabilized, whereas the LUMO becomes more destabilized, yielding the HOMO –1 and LUMO +1 in **1**-$D_3$ respectively. Concomitantly, the HOMO –1 and LUMO +1 of **1**-$C_2$ become more and less destabilized respectively, yielding the HOMO and LUMO of **1**-$D_3$. The net result is a widening of the band gap from –3.12 eV to –3.20 eV. This effect has also been reported for **HH,**[6] and computing of the frontier orbitals of **HBT** revealed a near identical effect (Fig. 3.10, Table S3.2), suggesting this "frontier orbital cross-over effect" to be a general feature of benzoid triphenylenes. It has been proposed this effect is the result of a greater planarity of propellerenes in their $D_3$ conformation.

For full comparison, computation of the FMOs of **5H** and **DBP** revealed a clear correlation between π-extension and size of the HOMO – LUMO gap, with an increase

and decrease in the HOMO and LUMO energy respectively, when going from **5H** to **1** and **HH** (Fig. S3.3); supporting the bathochromic shift observed in their UV-Vis spectra (Fig. 3.1).[38] Conversely, the near identical HOMO – LUMO gap of **1** *vis-à-vis* **HH** further confirms the notion that the position of π-extension is of lesser relevance than the fact of π-extension itself.

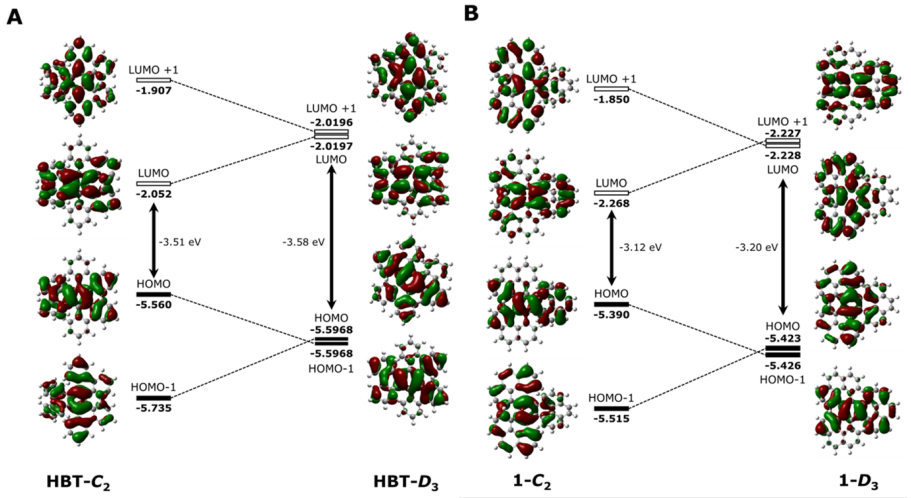


**Figure 3.10** Energy diagrams of the frontier orbitals of both enantiomers of **HBT** (A) and **1** (B) as computed at TDDFT-B3LYP/6-311+G(2d,p)//B3LYP-D3(BJ)/6-31G(d,p). Phases arbitrarily colored.

To conclude, it was shown that tripyrenylene **1** was isolated in a $C_2$ conformation. Computationally, this conformer was found to be thermodynamically less favorable, compared to the $D_3$ conformer. By computing the entire PES of the palladium catalyzed aryne trimerization used to synthesize it, it was shown that this reaction proceeds under kinetic control. This kinetic control could be pinpointed to the final aryne insertion step, which proceeds in a step-wise manner, rather than in a canonical Diels-Alder fashion. Using variable temperature NMR the conversion to the more stable isomer could be monitored. The spectroscopic properties of the separate isomers were then studied. Comparison of these properties to those of known helicenes, combined with a detailed FMO analysis, revealed that the position at which extension of the π-conjugated system is introduced is insignifcant, suggesting the helical motifs in these molecules to be dominant in dictating their photo-optical properties. Some initial evidence was found suggesting that the central ring of propellerenes may not be conjugated, something which has often be postulated based on computational models. Experiments are currently underway to validate these results.

**References**


(1) Kubo, H.; Hirose, T.; Matsuda, K. Control over the Emission Properties of [5]Helicenes Based on the Symmetry and Energy Levels of Their Molecular Orbitals. *Org. Lett.* **2017,** *19* (7), 1776.

(2) Griffiths, J. *Colour and constitution of organic molecules*; Academic press, **1976**.

(3) Fabian, J.; Hartmann, H. *Light absorption of organic colorants: theoretical treatment and empirical rules*; Springer Science & Business Media, 2013.

(4) Nishimoto, K. A MO theoretical study of organic dyes I. Effect of chemical softness on the electronic spectra. *Bull. Chem. Soc. Jap.* **1993,** *66* (7), 1876.

(5) Jenard-de Koninck, A.; Defay, N.; de Ridder, R. Synthèses dans le domaine des composés polycycliques aromatiques. XX. synthèses du 1,2-3,4-5,6-7,8-tétrabenzophénanthrène (ou tétrabenzo[a,c,g,i]phénanthrène) et du 1,12-2,3-10,11-tribenzopérylène (ou tribenzo[b,n,p,q,r]pérylène). *Bull. Soc. Chim. Belges* **1960,** *69* (11-12), 558.

(6) Hosokawa, T.; Takahashi, Y.; Matsushima, T.; Watanabe, S.; Kikkawa, S.; Azumaya, I.; Tsurusaki, A.; Kamikawa, K. Synthesis, structures, and properties of hexapole helicenes: Assembling six [5]helicene substructures into highly twisted aromatic systems. *J. Am. Chem. Soc.* **2017,** *139* (51), 18512.

(7) Rulíšek, L.; Exner, O.; Cwiklik, L.; Jungwirth, P.; Starý, I.; Pospíšil, L.; Havlas, Z. On the convergence of the physicochemical properties of [n] helicenes. *J. Phys. Chem. C* **2007,** *111* (41), 14948.

(8) Nakai, Y.; Mori, T.; Inoue, Y. Theoretical and experimental studies on circular dichroism of carbo [n] helicenes. *J. Phys. Chem. A* **2012,** *116* (27), 7372.

(9) The UV-Vis spectrum of dibenzo[f,j]picene was recorded in dioxane, all others in chloroform. However, inspection of the spectra suggests solvent effects to be negligible.

(10) Mori, T. Chiroptical properties of symmetric double, triple, and multiple helicenes. *Chem. Rev.* **2021,** *121* (4), 2373.

(11) Peña, D.; Cobas, A.; Pérez, D.; Guitián, E.; Castedo, L. Kinetic control in the palladium-catalyzed synthesis of $C_2$-symmetric hexabenzotriphenylene. A conformational study. *Org. Lett.* **2000,** *2* (11), 1629.

(12) Pozo, I.; Guitián, E.; Pérez, D.; Peña, D. Synthesis of nanographenes, starphenes, and sterically congested polyarenes by aryne cyclotrimerization. *Acc. Chem. Res.* **2019,** *52*(9), 2472-2481.

(13) Guitián, E.; Pérez, D.; Peña, D. In *Palladium in Organic Synthesis*; Springer, **2005**.

(14) Kluwer, A. M.; Elsevier, C. J.; Bühl, M.; Lutz, M.; Spek, A. L. Zero-valent palladium complexes with monodentate nitrogen σ-donor ligands. *Angew. Chem. Int. Ed.* **2003,** *42* (30), 3501.

(15) Hosokawa, T.; Asada, T.; Kamikawa, K. Theoretical examination of the plausible reaction process for stereoselective synthesis of hexapole helicene *via* a palladium-catalyzed [2+2+2] cyclotrimerization of [5]helicenyl aryne. *J. Phys. Chem. A* **2020,** *124* (4), 652.

(16) Schore, N. E. Transition metal-mediated cycloaddition reactions of alkynes in organic synthesis. *Chem. Rev.* **1988,** *88* (7), 1081.

(17) Examples of trimerization reactions which do not follow these two typical pathways are given in the preceding reference.

(18) Roglans, A.; Pla-Quintana, A.; Solà, M. Mechanistic studies of transition-metal-catalyzed [2+2+2] cycloaddition reactions. *Chem. Rev.* **2020**, *121*(3), 1894-1979.

(19) Retbøll, M.; Edwards, A. J.; Rae, A. D.; Willis, A. C.; Bennett, M. A.; Wenger, E. Preparation of benzyne complexes of group 10 Metals by intramolecular Suzuki coupling of *ortho*-metalated phenylboronic esters: Molecular structure of the first benzyne-palladium(0) complex. *J. Am. Chem. Soc.* **2002,** *124* (28), 8348.

(20) Marks, J. H.; Ward, T. B.; Brathwaite, A. D.; Ferguson, S.; Duncan, M. A. Cyclotrimerization of acetylene in gas phase $V^+(C_2H_2)_n$ complexes: Detection of intermediates and products with infrared spectroscopy. *J. Phys. Chem. A* **2019,** *123* (31), 6733.

(21) Given the sufficiently large barrier to interconversion of the two $D_3$ enantiomers their separation using chiral HPLC chromatography should be possible. Unfortunately, despite many attempts in this direction, such a separation was not found possible for **1**-$D_3$.
(22) Förster, T.; Kasper, K. Ein konzentrationsumschlag der fluoreszenz des pyrens. *Z. Elektrochem.* **1955,** *59* (10), 976.
(23) Stevens, B. Evidence for the photo-association of aromatic hydrocarbons in fluid media. *Nature* **1961,** *192* (4804), 725.
(24) Birks, J. B.; Christophorou, L. G. Excimer fluorescence spectra of pyrene derivatives. *Spectrochimica Acta* **1963,** *19* (2), 401.
(25) Hanlon, A. D.; Milosavljevic, B. H. Appropriate excitation wavelength removes obfuscations from pyrene excimer kinetics and mechanism studies. *Photochemical & Photobiological Sciences* **2013,** *12* (5), 787.
(26) Birks, J. B. Excimers. *Rep. Prog. Phys.* **1975,** *38* (8), 903.
(27) Winnik, F. M. Photophysics of preassociated pyrenes in aqueous polymer solutions and in other organized media. *Chem. Rev.* **1993,** *93* (2), 587.
(28) Förster, T. Excimers and exciplexes. *The Exciplex. Academic, New York* **1975**, 1.
(29) Okamoto, Y.; Nakamura, M.; And, M. S.; Takamuku, S. Formation of intramolecular excimer in aryl phosphates and their reactivities. *Photochem. Photobiol.* **1992,** *56* (3), 403.
(30) Turro, N. J. *Modern molecular photochemistry*; University science books, 1991.
(31) Birks, J. B.; Christophorou, L. G. Excimer fluorescence of aromatic hydrocarbons in solution. *Nature* **1962,** *194* (4827), 442.
(32) Hirayama, F. Intramolecular excimer formation. I. Diphenyl and triphenyl alkanes. *J. Chem. Phys.* **1965,** *42* (9), 3163.
(33) Fernandez, I.; Frenking, G. Direct estimate of conjugation and aromaticity in cyclic compounds with the EDA method. *Faraday Discuss.* **2007,** *135*, 403.
(34) Pierrefixe, S. C. A. H.; Bickelhaupt, F. M. Aromaticity: molecular-orbital picture of an intuitive concept. *Chem. Eur. J.* **2007,** *13* (22), 6321.
(35) Roy, M.; Berezhnaia, V.; Villa, M.; Vanthuyne, N.; Giorgi, M.; Naubron, J. V.; Poyer, S.; Monnier, V.; Charles, L.; Carissan, Y. Stereoselective syntheses, structures, and properties of extremely distorted chiral nanographenes embedding hextuple helicenes. *Angew. Chem. Int. Ed.* **2020,** *59* (8), 3264.
(36) Antić, M.; Furtula, B.; Radenkovic, S. Aromaticity of nonplanar fully benzenoid hydrocarbons. *J. Phys. Chem. A* **2017,** *121* (18), 3616.
(37) Hosokawa, T.; Tsurusaki, A.; Kamikawa, K. Assembly of [5]helicene subunits by palladium-catalyzed reactions: Synthesis, structures, properties, and theoretical study of multiple helicenes. *J. Synth. Org. Chem. Jap.* **2020,** *78* (11), 1013.
(38) Wade, L. G. Conjugated systems, orbital symmetry, and ultraviolet spectroscopy. *Organic chemistry. Englewood Cliffs, NJ: Prentice Hall* **1991**, 667.
(39) Pena, D.; Pérez, D.; Guitián, E.; Castedo, L. Synthesis of hexabenzotriphenylene and other strained polycyclic aromatic hydrocarbons by palladium-catalyzed cyclotrimerization of arynes. *Org. Lett.* **1999,** *1* (10), 1555.
(40) Adachi, K.; Hirose, S.; Ueda, Y.; Uekusa, H.; Hamura, T. Thermodynamically stable *o*-quinodimethane: Synthesis, structure, and reactivity. *Chem. Eur. J.* **2020**, *27* (11), 3665-3669.
(41) Frisch, M. J.; Trucks, G. W.; Schlegel, H. B.; Scuseria, G. E.; Robb, M. A.; Cheeseman, J. R.; Scalmani, G.; Barone, V.; Mennucci, B.; Petersson, G. A. Gaussian 09 Revision D. 01, 2009. *Gaussian Inc. Wallingford CT* **2009**.
(42) PBE was used as both exchange and correlation functional, and was called using the pbepbe keyword in the Gaussian 09 software. At the DFT-D3(BJ) level of theory the s6 and s8 values are set to 1 and 0.7875 respectively, whereas the ABJ1 and ABJ2 values are set respectively to 0.4289 and 4.4407.
(43) Grimme, S.; Antony, J.; Ehrlich, S.; Krieg, H. A consistent and accurate ab initio parametrization of density functional dispersion correction (DFT-D) for the 94 elements H-Pu. *J. Chem. Phys.* **2010,** *132* (15), 154104.

(44) Grimme, S.; Ehrlich, S.; Goerigk, L. Effect of the damping function in dispersion corrected density functional theory. *J. Comp. Chem.* **2011,** *32* (7), 1456.
(45) Hay, P. J.; Wadt, W. R. Ab initio effective core potentials for molecular calculations. Potentials for K to Au including the outermost core orbitals. *J. Chem. Phys.* **1985,** *82* (1), 299.
(46) Marenich, A. V.; Cramer, C. J.; Truhlar, D. G. Universal solvation model based on solute electron density and on a continuum model of the solvent defined by the bulk dielectric constant and atomic surface tensions. *J. Phys. Chem. B* **2009,** *113* (18), 6378.
(47) Bootsma, A. N.; Wheeler, S. E. Popular integration grids can result in large errors in DFT-computed free energies. *ChemRxiv. Preprint* **2019**.
(48) Ribeiro, R. F.; Marenich, A. V.; Cramer, C. J.; Truhlar, D. G. Use of solution-phase vibrational frequencies in continuum models for the free energy of solvation. *J. Phys. Chem. B* **2011,** *115* (49), 14556.
(49) Funes-Ardoiz, I.; Paton, R. S. (2016). GoodVibes: GoodVibes v1.0.2. http://doi.org/10.5281/zenodo.595246.
(50) Legault, C. Y. *CYLview, 1.0 b, Université de Sherbrooke, 2009*, 2013.
(51) Vacek, J.; Hrbáč, J.; Strašák, T.; Církva, V.; Sýkora, J.; Fekete, L.; Pokorný, J.; Bulíř, J.; Hromadová, M.; Crassous, J. Anodic deposition of enantiopure hexahelicene layers. *ChemElectroChem* **2018,** *5* (15), 2080.
(52) Kashihara, H.; Asada, T.; Kamikawa, K. Synthesis of a double helicene by a palladium-catalyzed cross-coupling reaction: Structure and physical properties. *Chem. Eur. J.* **2015,** *21* (17), 6523.
(53) Bédard, A. C.; Vlassova, A.; Hernandez-Perez, A. C.; Bessette, A.; Hanan, G. S.; Heuft, M. A.; Collins, S. K. Synthesis, crystal structure and photophysical properties of pyrene–helicene hybrids. *Chem. Eur. J.* **2013,** *19* (48), 16295.
(54) Saito, H.; Uchida, A.; Watanabe, S. Synthesis of a three-bladed propeller-shaped triple [5]Helicene. *J. Org. Chem.* **2017,** *82* (11), 5663.
(55) Sakai, H.; Kubota, T.; Yuasa, J.; Araki, Y.; Sakanoue, T.; Takenobu, T.; Wada, T.; Kawai, T.; Hasobe, T. Synthetic control of photophysical process and circularly polarized luminescence of [5]carbohelicene derivatives substituted by maleimide units. *J. Phys. Chem. C* **2016,** *120* (14), 7860.

## Experimental

*General*. All reagents were obtained from commercial sources and were used as received. Hexabenzotriphenylene was synthesized according to known procedures.[11,39] Solvents used were stored over 4 Å molecular sieves. Reactions were monitored by TLC analysis using Merck 25 DC plastikfolien 60 F254 with detection by using an aqueous solution of $KMnO_4$ (7%) and $K_2CO_3$ (2%) followed by charring at ~150 °C. Column chromatography was performed on Fluka silica gel (0.04–0.063 mm). High-resolution mass spectra were recorded by direct injection (2 µL of a 2 µM solution in water/acetonitrile; 50:50; v/v and 0.1% formic acid) on a mass spectrometer (Thermo Finnigan LTQ Orbitrap) equipped with an electrospray ion source in positive mode (source voltage 3.5 kV, sheath gas flow 10, capillary temperature 250 °C). The high-resolution mass spectrometer was calibrated prior to measurements with a calibration mixture (Thermo Finnigan). All NMR experiments were performed on a Bruker AV500 NMR instrument equipped with a BBFO probe head for 5 mm outer diameter tubes. Spectra were recorded at 500 MHz for $^1$H, 125 MHz for $^{13}$C and 470 MHz for $^{19}$F. All deuterated solvents were obtained from a commercial source (Eurisotop) and were used as received. Chemical shifts are given in ppm (δ) relative to TMS (0 ppm), and coupling constants (*J*) are given in Hertz (Hz).

**Tripyrenylene 1-*C*$_2$**

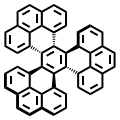

$^1$H NMR (500 MHz, Tol-$d_8$) δ 8.43 (d, *J* = 8.0 Hz, 1H), 7.87 (dd, *J* = 7.5, 1.0 Hz, 1H), 7.85 (s, 1H), 7.40 (t, *J* = 7.5 Hz, 1H).

**Tripyrenylene 1-*D*$_3$**


A solution of **1-*C*$_2$** in toluene was heated to 80 °C for 5 hours, resulting in the formation of a bright yellow precipitate. The solvent was removed under reduced pressure to yield the desired product. $^1$H NMR (500 MHz, $CS_2$:DCM-$d_2$) δ 8.29 (d, *J* = 8.0 Hz, 1H), 8.11 (dd, *J* = 7.5, 1.0 Hz, 1H), 8.12 (s, 1H), 7.57 (t, *J* = 7.5 Hz, 1H).

**10-Bromo-9-phenanthrol (2)**[40]

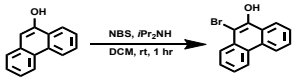


Commercial 9-phenanthrol was purified by column chromatography over silica gel using EtOAc:Pentane (1:25) as eluent and used immediately. The 9-phenanthrol (1.57 g, 8.1mmol) was dissolved in DCM (50 mL) together with *i*Pr$_2$NH (0.1 mL, 0.7 mmol). A solution of NBS (1.44 g, 8.1mmol) in DCM (50 mL) was then added dropwise over 30 min on ice. After addition was complete, the mixture was stirred for another 3 hours. The reaction mixture was then poured onto $H_2O$ (100 mL), and acidified to pH 1 by the addition of a few drops of concentrated $H_2SO_4$. The resulting mixture was extracted with DCM, and the combined organic layers were dried over anhydrous $Na_2SO_4$, filtered, and concentrated under reduced pressure. Column chromatography of the residue (1:20 EtOAc:Pentane) afforded the desired compound as a pale-yellow solid (1.79 g, 6.55 mmol, 81.1%). $^1$H NMR (500Mz, $CDCl_3$) 8.67-8.61 (m, 2), 8.39 (dd, *J* = 1.5, 13.0 Hz, 1H), 8.14 (dd, *J* = 1.5, 13.5 Hz, 1H), 7.75-7.69 (m, 1H), 7.68-7.63 (m, 1H), 7.59-7.56 (m, 1H), 6.30 (s, 1H).

**10-(trimethylsilyl)phenanthren-9-yl trifluoromethanesulfonate (3)**

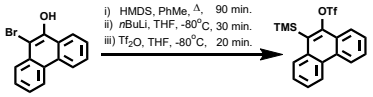


A solution of 10-bromo-9-phenanthrol (0.476 g, 1.74 mmol) and HMDS (0.4 mL, 1.92 mmol) in THF (6 mL) was refluxed for 90 minutes. The solvent and excess reagent were then removed under reduced pressure, the residue redissolved in THF (12 mL) and the solution cooled to -80°C using an Ace:liquid $N_2$ bath. Then, *n*-BuLi in hexanes (1.83 mL, 2.46 M, 1.83 mmol) was added dropwise and stirring continued for 30 minutes before $Tf_2O$ (0.37 mL, 2.18 mmol) was added in one portion. Stirring was continued for 20 min. and the reaction then quenched by the addition of cold sat. $NaHCO_3$. The layers were separated, the aqueous layer extracted with $Et_2O$, and the combined organic layers dried over $Na_2SO_4$, filtered and concentrated under reduced pressure. Column chromatography over silica gel ($Et_2O$–hexane, 1:99) afforded the product (0.2 g, 30%) as a colourless oil. $^1$H NMR (500MHz, $CDCl_3$) δ 8.70-8.66 (m, 2H), 8.27 (dd, 8.00, 1.5 Hz, 1H), 8.19 (dd, 8.00, 1.5 Hz, 1H), 7.75-7.66 (m, 4H), 0.67 (s, 9H). $^{13}$C NMR (125MHz, $CHCl_3$) δ 134.78, 132.91, 130.65, 130.12, 129.86, 128.51, 127.44, 127.33, 126.77, 125.94, 123.47, 122.88, 122.36, 118.92 (q, $^1J_{CF}$ = 320.7Hz), 2.38. $^{19}$F NMR (470MHz, $CDCl_3$) δ -72.61.

**Hexabenzotriphenylene-*C*$_2$ (HBT)**

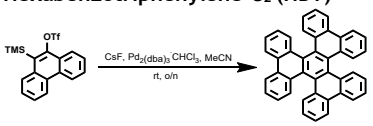


The oil obtained above was dissolved in dry MeCN (10 mL) together with $Pd_2(dba)_3{\cdot}CHCl_3$ (28 mg, 0.026 mmol). Then, finely powdered anhydrous CsF (244 mg, 1.6 mmol) was added and the mixture stirred at room temperature overnight under a dry $N_2$ atmosphere. The suspension was filtered, and the residue washed with MeCN (5 mL) and $Et_2O$ (1 mL) and dried under vacuum to afford the title compound as a yellow solid. Yield: 7 mg, 21%. $^1$H NMR (500 MHz, DCM-$d_2$) δ 8.65 (d, *J* = 8.0 Hz, 6H), 8.20 (d, *J* = 8.5 Hz, 6H), 7.64 (ddd, J = 8.2, 6.9, 1.2 Hz, 6H), 7.29 (m, 6H). The $C_2$ conformer was converted to the $D_3$ conformer as described for **1**. $^1$H NMR (500 MHz, $CDCl_3$) δ 8.54 (d, *J* = 7.5 Hz, 6H), 8.16 (d, *J* = 8.0 Hz, 6H), 7.57 – 7.52 (m, 6H), 7.23 – 7.19 (m, 6H).

*VT NMR experiments.* All variable temperature experiments NMR experiments were performed on a Bruker AV500 NMR instrument equipped with a BBFO probe head for 5 mm outer diameter tubes. Spectra were recorded at 500 MHz for $^1$H. To determine the $C_2 \rightarrow D_3$ interconversion barrier height, a solution of pyrene propeller-$C_2$ in toluene-$d_8$ was heated to 80 °C and kept at this temperature. The decrease in signal intensity of resonances corresponding to the $C_2$ conformer, relative to that of residual solvent signal, was monitored over time. Barrier heights were then derived from the signal decrease half time $t_{½}$ using the Eyring equation:

$$k = \frac{k_b T}{h} e^{-\frac{\Delta G^{\ddagger}}{RT}};\ t_{1/2} = \frac{\ln(2)}{k}$$

where $k$ is the rate constant in sec$^{-1}$, $k_b$ is Boltzmann's constant, $T$ is the absolute temperature, $h$ is Planck's constant, $R$ is the universal gas constant and the transmission coefficient has been set to 1 and has thus been omitted. For the $^1C_2 \leftrightarrow {}^2C_2$ interconversion barrier heights solutions of pyrene propeller $C_2$ in toluene-$d_8$ were cooled and the barrier height derived from the coalescence temperature ($T_c$) as:

$$\Delta G^{\ddagger} = RT_c \left[23 + \frac{T_c}{\Delta \nu}\right]$$

where $\Delta\nu$ is the coupling constant in Hertz.

*Computational*. Equilibrium geometries of all structures were computed at the DFT level of theory using the Gaussian 09 Rev. D.01 program,[41] using the PBE functional[42] and 6-31G(d,p) basis set and D3(BJ) dispersion correction.[43,44] For structures containing Pd atoms the LANL2DZ (with effective core potential) basis set was used on Pd and a 6-31G(d,p) basis set on all other atoms.[45]Geometries were optimized in the gas-phase and subsequently re-optimized in combination with the SMD model to include solvent effects, using acetonitrile as the solvent parameter.[46] For the time-dependent (TD) DFT computations, geometries were first optimized in the gas-phase using the B3LYP functional, 6-31G(d,p) basis set and D3(BJ) dispersion correction, and TD computations then performed using the same functional but using the larger 6-311+G(2d,p) basis set. For all computations the convergence criteria were set to tight (Opt = tight; Max. Force = $1.5 \cdot 10^{-7}$, Max. Displacement = $6.0 \cdot 10^{-7}$), and an internally defined super-fine grid size was used (SCF = tight, Int = VeryFineGrid), which is a pruned 175,974 grid for first-row atoms and a 250,974 grid for all other atoms.[47] These parameters were chosen because of the significant dependence of computed frequencies on the molecular orientation when using smaller grid sizes. This effect was particularly pronounced for transition metals and transition state structures.[47]

Denoted free Gibbs energies were computed using Equation S1, in which $\Delta E_{gas}$ is the gas-phase energy (electronic energy), $\Delta G^{T}_{gas,QH}$ ($T$ = 293.15 K, $p$ = 1 atm., $C$ = 1 M) is the sum of corrections from the electronic energy to the free Gibbs energy in the quasi-harmonic oscillator approximation, including zero-point-vibrational energy, and $\Delta G_{solv}$ is their corresponding free solvation Gibbs energy. The $\Delta G^{T}_{gas,QH}$ were computed using the quasi-harmonic approximation in the gas phase according to the work of Truhlar - the quasi-harmonic approximation is the same as the harmonic oscillator approximation except that vibrational frequencies lower than 100 cm$^{-1}$ were raised to 100 cm$^{-1}$ as a way to correct for the breakdown of the harmonic oscillator model for the free energies of low-frequency vibrational modes.[48,49] All stationary points found were checked for either no imaginary frequencies for local minima or one imaginary frequency for transition state structures.

$$\begin{aligned} \Delta G^{T}_{solv} &= \Delta E_{gas} + \Delta G^{T}_{gas,QH} + \Delta G_{solv} \\ &= \Delta G^{T}_{gas} + \Delta G_{solv} \end{aligned} \qquad \text{(Eq. S1)}$$

Transition states for the propellerene interconversion were obtained by first performing a dihedral angle scan in the Gaussian software to provide guess structures for a QST3 search.

Transition states in the palladium(0) catalyzed reactions were obtained using a QST2 search. The obtained guess structures were optimized to a transition state using the Berny algorithm and confirmed by an intrinsic reaction coordinate calculation. Frontier orbitals were computed using TDDFT at the B3LYP/6-311+G(2d,p) level, using geometries optimized at the SMD($CHCl_3$)-B3LYP-D3(BJ)/6-31G(d,p) level of theory. Molecular structures were illustrated using CYLview.[50]

## Supplementary Figures and Tables

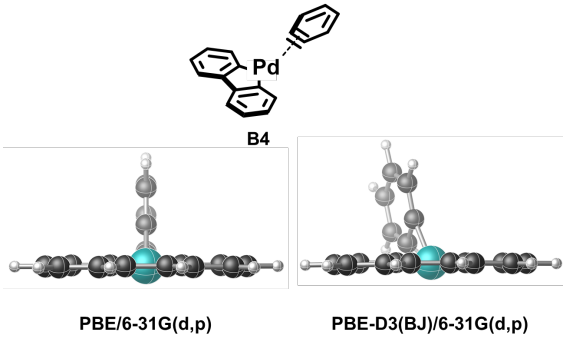


**Figure S3.1.** Computed gas-phase geometries of the **B4** complex, optimized without and with D3(BJ) dispersion correction.

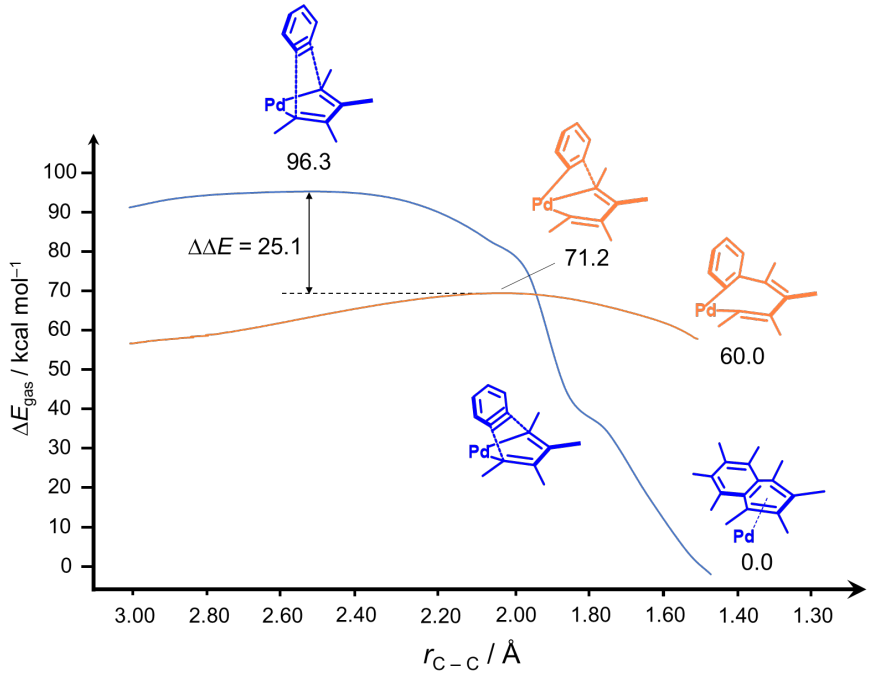


**Figure S3.2** Potential energy surfaces for the step-wise addition (orange) and concerted synchronous addition (blue) of **P3**···phenanthr-4,5-yne complexes. Reported are gas-phase electronic energies (kcal $mol^{-1}$) projected unto the bond forming C – C distances (dashed lines in structures) at PBE-D3(BJ)/6-31G(d,p). Structures are drawn in abbreviated form for clarity.

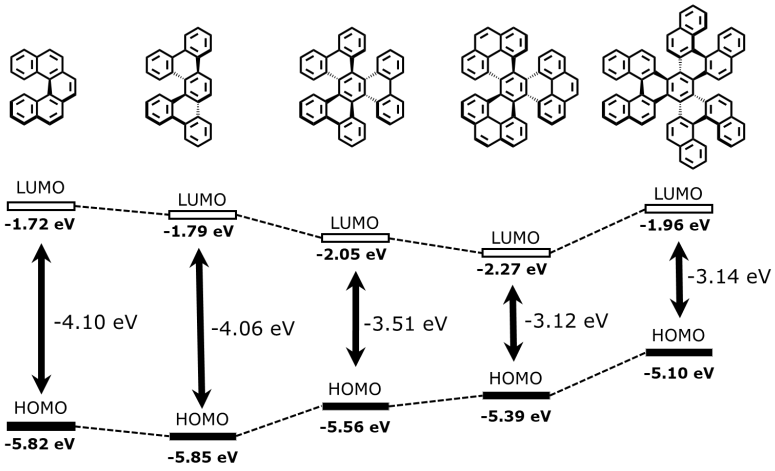


**Figure S3.3** Energy diagram of the FMOs of helicenes and propellerenes computed at the B3LYP-D3(BJ)/6-311+G(2d,p)//B3LYP-D3(BJ)/6-31G(d,p) level of theory.

**Table S3.1** Computed HOMO – LUMO energies of [5]helicene at different levels of theory, and the experimental HOMO energy level, in eV.

| | **1** | **2** | **3** | **4** | **5** | **6** |
|---|---|---|---|---|---|---|
| LUMO | | -1.72 | -1.85 | -2.08 | -1.34 | -1.29 |
| HOMO | -5.81 | -5.82 | -5.97 | -5.49 | -5.53 | -5.49 |
| gap | | -4.10 | -4.12 | -3.41 | -4.19 | -4.20 |

**1** Experimental value[51]
**2** B3LYP/6-311+G(2d,p)//B3LYP-D3(BJ)/6-31G(d,p) [This Work]
**3** PCM(ACN)B3LYP/6-311++G(d,p)[51]
**4** M06-2X/6-31+G(d,p)//PCM(Acetone)B3LYP/6-31G(d,p)[52]
**5** IEFPCM(DCM)B3LYP/6-31G(d)[53]
**6** B3LYP/6-31G(d)[54,55]

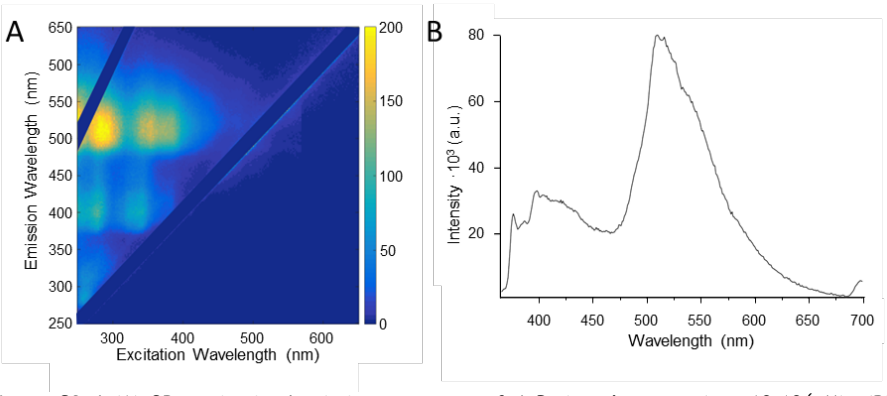


**Figure S3.4** (A) 2D excitation/emission spectrum of **1**-$D_3$ in *n*-heptane ($c$ = $10 \cdot 10^{-6}$ M). (B) Emission spectrum of **1**-$D_3$ in *n*-heptane:$CHCl_3$, excited at 350 nm.

**Table S3.2** Transition energies, wavelengths, and oscillator strengths (*f*) of benzoid triphenylenes as computed at the TDDFT/B3LYP/6-311+G(2d,p)//SMD($CHCl_3$)-B3LYP-D3(BJ)/6-31G(d,p) level of theory. HOMO → LUMO transitions are shaded in grey.

**HBT-C2**

HOMO = 138; LUMO = 139

| | | |
|---|---|---|
| Excited State 1: | | Singlet-A |
| 2.9039 eV | 426.95 nm | f=0.0002 |
| 137 -> 139 | | 0.51513 |
| 138 -> 140 | | 0.47924 |
| Excited State 2: | | Singlet-A |
| 3.0329 eV | 408.79 nm | f=0.0666 |
| 137 -> 140 | | -0.22871 |
| 138 -> 139 | | 0.66124 |
| Excited State 3: | | Singlet-A |
| 3.3879 eV | 365.96 nm | f=0.2998 |
| 137 -> 140 | | 0.62936 |
| 138 -> 139 | | 0.21034 |
| 138 -> 141 | | 0.18027 |

**HBT-D3**

HOMO = 138; LUMO = 139

| | | |
|---|---|---|
| Excited State 1: | | Singlet-A |
| 2.8021 eV | 442.47 nm | f=0.0000 |
| 137 -> 139 | | 0.46261 |
| 137 -> 140 | | -0.18357 |
| 138 -> 139 | | 0.18361 |
| 138 -> 140 | | 0.46256 |
| Excited State 2: | | Singlet-A |
| 3.0157 eV | 411.13 nm | f=0.0284 |
| 137 -> 139 | | -0.18273 |
| 137 -> 140 | | -0.46008 |
| 138 -> 139 | | 0.46046 |
| 138 -> 140 | | -0.18261 |
| Excited State 3: | | Singlet-A |
| 3.2555 eV | 380.85 nm | f=0.4477 |
| 137 -> 139 | | -0.45234 |
| 137 -> 140 | | -0.18099 |
| 138 -> 139 | | -0.18094 |
| 138 -> 140 | | 0.45236 |

**1-C2**

HOMO = 156; LUMO = 157

| | | |
|---|---|---|
| Excited State 1: | | Singlet-A |
| 2.6500 eV | 467.87 nm | f=0.0001 |
| 155 -> 157 | | 0.53026 |
| 156 -> 158 | | -0.45459 |
| Excited State 2: | | Singlet-A |
| 2.7487 eV | 451.06 nm | f=0.0606 |
| 154 -> 157 | | -0.21271 |
| 156 -> 157 | | 0.66093 |
| Excited State 3: | | Singlet-A |
| 2.9217 eV | 424.36 nm | f=0.0097 |
| 154 -> 157 | | 0.58276 |
| 155 -> 158 | | 0.33993 |
| 156 -> 157 | | 0.14427 |

**1-D3**

HOMO = 156; LUMO = 157

| | | |
|---|---|---|
| Excited State 1: | | Singlet-A |
| 2.5687 eV | 482.68 nm | f=0.0000 |
| 155 -> 157 | | -0.49269 |
| 156 -> 158 | | 0.49624 |
| Excited State 2: | | Singlet-A |
| 2.7860 eV | 445.03 nm | f=0.0264 |
| 155 -> 158 | | 0.47977 |
| 156 -> 157 | | 0.49734 |
| Excited State 3: | | Singlet-A |
| 2.8694 eV | 432.09 nm | f=0.1988 |
| 154 -> 157 | | -0.33192 |
| 155 -> 157 | | 0.43049 |
| 156 -> 158 | | 0.42769 |
| 156 -> 159 | | 0.13314 |